Materials Advances

ROYAL SOCIETY OF CHEMISTRY

PAPER

View Article Online
View Journal | View Issue

Check for updates

Cite this: *Mater. Adv.*, 2020, 1, 908

A yolk–albumen–shell structure of mixed Ni–Co oxide with an ultrathin carbon shell for high-sensitivity glucose sensors†

Xuan Zhang, [ab] Yawei Zhang,[b] Wei Guo,[a] Kai Wan, [a] Ting Zhang,[c] Jordi Arbiol, *[cd] Yong-Qing Zhao, [e] Cai-Ling Xu, [e] Maowen Xu *[b] and Jan Fransaer*[a]

Received 22nd April 2020,
Accepted 16th June 2020

DOI: 10.1039/d0ma00230e

rsc.li/materials-advances

Non-enzymatic glucose sensors based on different Co–Ni–C composite materials were developed by pyrolysis of bimetallic or single metal based metal–organic frameworks (MOFs). The structure and composition of the resulting materials were explored by XRD, nitrogen adsorption/desorption isotherms, SEM, HRTEM and STEM-EELS. The electrochemical performance of the bimetallic MOF derived novel yolk–albumen–shell structure of Ni–Co@C (YASNiCo@C) stands out from these materials. The YASNiCo@C electrode exhibited a sensitivity of 1964 μA cm^{-2} mM^{-1} with the detection limit of 0.75 μM, a linear range from 5 μM to 1000 μM and good stability for the detection of glucose. These promising electrochemical performances prove that YASNiCo@C is a promising material for glucose sensors. Moreover, the strategy outlined in this work for the design of MOF based nanomaterials can also be used beyond glucose sensors.

1. Introduction

Detection of glucose is widely used in the food industry, medical diagnosis and environmental monitoring. The development of high sensitivity and low-cost glucose sensors is highly desirable for the broad academic community and industry. Even though many techniques can be used for the detection of glucose, electrochemical sensors dominate the market because of their sensitivity, reproducibility and low cost.

Generally speaking, there are two kinds of electrochemical sensors of glucose: enzymatic and non-enzymatic. Since the 1960s, when the first enzyme electrode was described,[1,2] many efforts have been made to use enzymatic biosensors and three generations of glucose sensors have been successfully developed based on glucose oxidase (GOx). The first generation glucose sensor relied on the use of the natural oxygen co-substrate and generation with indirect detection of glucose by detecting hydrogen peroxide.[3] Due to the oxygen dependence and high operating potential of the first generation glucose sensor, the second generation glucose sensors based on the immobilization of GOx on a redox mediator were developed, which solved the problem of oxygen dependence.[4,5] In order to eliminate the mediator, the third generation of glucose sensors uses direct electron transport between the immobilized enzymes and the electrode surface. However, the third generation glucose sensors still suffer from low stability, low sensitivity and small linear range.[6] More importantly, all these enzymatic sensors are affected by the intrinsic properties of the GOx, which is affected by temperature (<40 °C), pH (2–8) and humidity. These drawbacks strongly hinder the glucose sensor applications in the food industry, environment monitoring, fuel cells and operating batteries. A fourth generation glucose sensor based on non-enzymatic electrodes, constructed out of active metal-based nanoparticles, is considered as a good candidate for these applications.

Different transition metal (Cu, Ni, Fe, Co, Mn, *etc.*) oxides have been explored as fourth-generation glucose sensor materials due to their high sensitivity and low cost.[7–9] Among these transition metals, Co and Ni show superior electrocatalytic

[a] *Department of Materials Engineering, KU Leuven, Leuven 3001, Belgium. E-mail: jan.fransaer@kuleuven.be*
[b] *Key Laboratory of Luminescent and Real-Time Analytical Chemistry (Southwest University), Ministry of Education, School of Materials and Energy, Southwest University, Chongqing 400715, P. R. China. E-mail: xumaowen@swu.edu.cn*
[c] *Catalan Institute of Nanoscience and Nanotechnology (ICN2), CSIC and BIST, Campus UAB, Bellaterra, 08193 Barcelona, Catalonia, Spain. E-mail: arbiol@icrea.cat*
[d] *ICREA, Pg. Lluís Companys 23, 08010 Barcelona, Catalonia, Spain*
[e] *State Key Laboratory of Applied Organic Chemistry, Key Laboratory of Nonferrous Metal Chemistry and Resources Utilization of Gansu Province, Laboratory of Special Function Materials and Structure Design of the Ministry of Education, College of Chemistry and Chemical Engineering, Lanzhou University, Lanzhou, 730000, China*

† Electronic supplementary information (ESI) available. See DOI: 10.1039/d0ma00230e

activity and high stability toward electro-oxidation of glucose in alkaline media.[10–13] In order to increase the electrocatalytic active surface area of these active materials, different kinds of nanostructures have been used for glucose electrocatalysis, such as nanowires,[13] nanosheets,[14] nanodisks, nanorods,[15] nanotubes,[16] nanoflowers[17] and so on. However, the poor electrical conductivity of these metal oxides and their tendency to aggregate has hindered their applications. The combination of metal oxides and carbon materials is a promising way to solve these problems, which could be beneficial for the activity, selectivity, and durability of such glucose sensors.[18–23] For example, Junhong Chen *et al.* prepared CoO/graphene microsphere hybrid materials for glucose sensors.[24] Compared to pure CoO electrodes, CoO/graphene electrodes showed around 2 times higher current response for 0.1 mM glucose with a sensitivity of 670 μA mM^{-1} cm^{-2}.

To increase the effective surface area and enhance the mass and ion transport of these nanomaterials, the construction of porous carbon–metal oxide nanomaterial composite materials *via* pyrolysis of metal–organic frameworks (MOFs) has drawn extensive attention. These materials have been used for batteries,[25,26] supercapacitors,[27,28] solar cells[29,30] and catalysis[31–35] applications. Recently, this method was also used to prepare materials for glucose sensors. Minbo Lan *et al.* pyrolyzed ZIF-67 in different atmospheres (air and nitrogen) at 700 °C to prepare cobalt nanoparticles-porous carbon composites materials.[36] The sensitivity of ZIF-67 derived CoO/carbon composite materials (pyrolyzed under nitrogen) showed a sensitivity of 227 μA mM^{-1} cm^{-2} (10 times higher than pyrolyzed under air), and a linear range of 0.1–1.1 mM with a limit of detection of 6 μM. Compared with single metal-based electrodes, bimetallic compounds often show higher sensitivity.[37,38] For example, G. Gnana Kumar *et al.* synthesized CuO/NiO–carbon nanocomposite materials by the pyrolysis of Cu–Ni MOFs.[39] Compared to the pure Cu–carbon based or Ni–carbon based materials, CuO/NiO–carbon nanocomposite materials had a considerable current response for 5 mM glucose (around 1.5 times higher than CuO/C and 1.2 times higher than NiO/C nanocomposite materials) with a sensitivity of 587 μA mM^{-1} cm^{-2}. However, MOFs that have uniformly distributed metals ion of nodal positions often suffer from the fragile frameworks due to the introduction of second metal nodes.[40–45] To the best of our knowledge, even though mixed Co–Ni metal oxides are considered as one of the most active materials for glucose sensors,[37,38] preparation of the mixed Co–Ni metal oxides for glucose sensors *via* pyrolysis of bimetallic MOFs has been rarely reported.

In this work, Co–Ni bimetallic MOFs with a uniform distribution of the nodal positions were synthesized. After pyrolysis, different compositions and structures of Co–Ni metal oxide with ultrathin carbon shell materials were prepared. The resulting materials were used to fabricate non-enzymatic electrochemical glucose sensor electrodes. Among these electrodes, the bimetallic MOF-derived materials displayed much better electrochemical catalytic performance towards glucose than materials based on pure Co or Ni MOFs.

2. Results and discussion

The Co–Ni composite materials were synthesized by the pyrolysis of bimetallic Co–Ni MOFs as shown in Fig. 1. For M(HBTC)(4,4′-bipy) (M = Ni, Co or mixture of Co and Ni), the coordination environment of the metal centers is bound by three BTC units with one bidentate carboxylic group and two monodentate carboxylic groups, forming a layered structure with honeycomb pores. The polar positions on the nickel(II) or cobalt(II) centers are occupied by 4,4′-bipyridine along the *c* axis to form a stable 3D framework. The morphologies and compositions of these MOFs are characterized by SEM. In order to evaluate the elemental distribution of Ni/Co, electron probe microanalysis (EPMA) coupled with wavelength dispersive spectroscopy (WDS) was used for determination of metal element compositions, which has more sensitivity than energy dispersive spectroscopy (EDS).[46] As shown in Fig. 2, all the samples have similar hexagonal sheet-like morphology. For Co–Ni bimetallic MOFs, the distribution of Ni and Co in the hexagonal sheets is fairly homogeneous. The ratio between Co and Ni is around 1 : 1, which is in good agreement with the ICP results (1.06 : 1). The crystallinity of the as-prepared MOFs and the corresponding metal oxide–carbon composite materials is characterized by XRD (Fig. 3 and Fig. S1, ESI†). All these MOFs have similar XRD patterns as they possess the same crystal structure, indicating the successful incorporation of a second metal into the frameworks. The powder XRD patterns show clear characteristic diffraction peaks at $2\theta \approx 7.8°$, 10.6°, 15.6° and 18.5°, which match well with the simulated patterns.[47]

The thermal stabilities of the pristine MOFs were explored by thermal gravimetric analysis (TGA) under an argon atmosphere (Fig. 4a). The TGA curves showed two weight-loss steps.

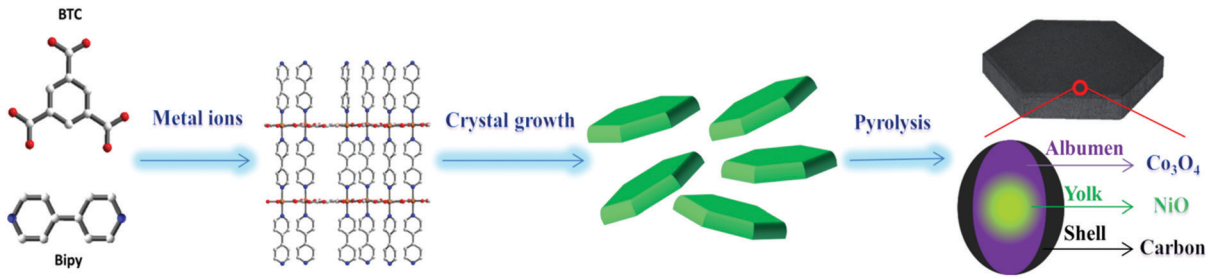

Fig. 1 Schematic illustration of the synthesis of YASNiCo@C.

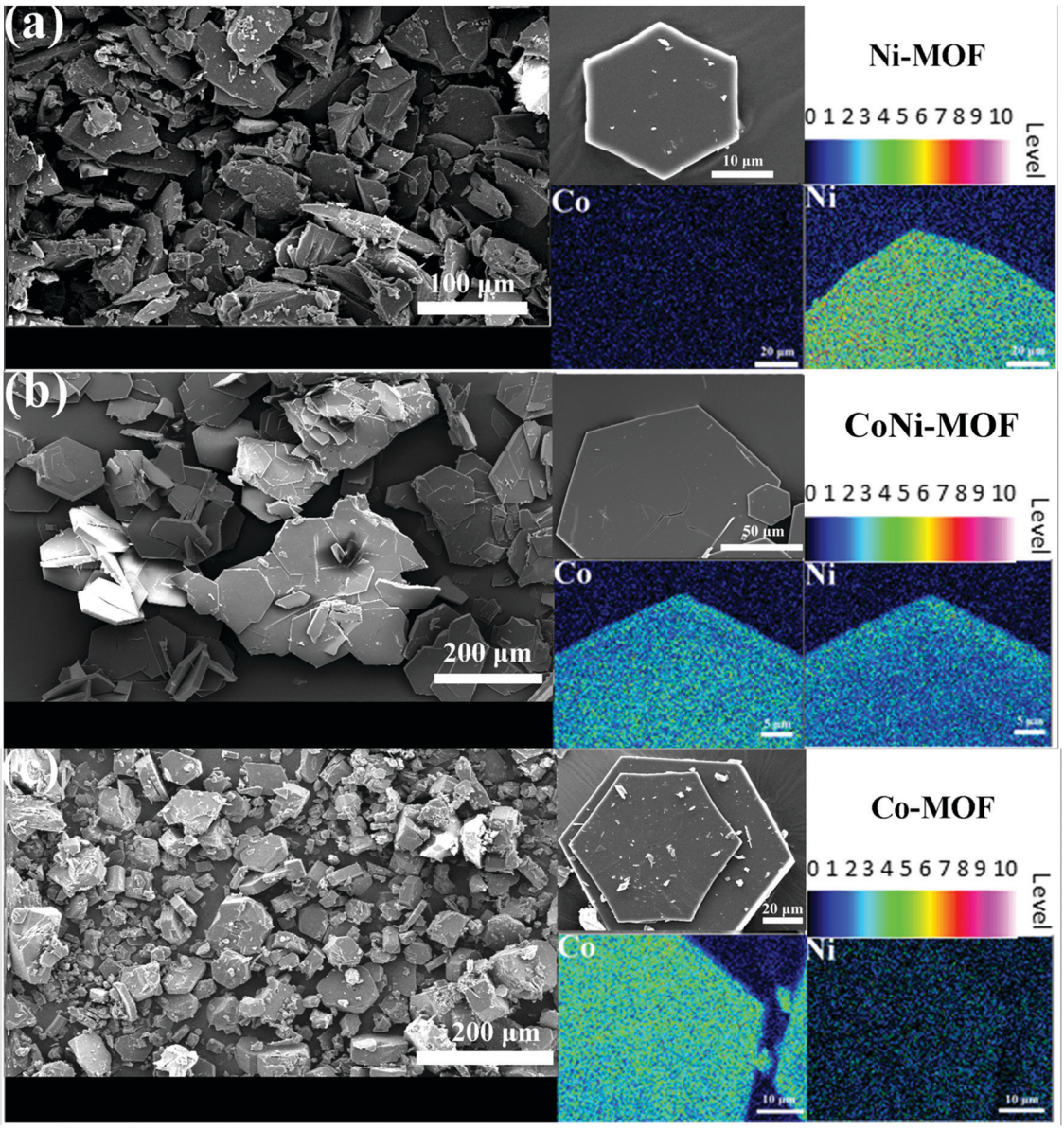

Fig. 2 SEM images of different MOFs and the corresponding EMPA elemental mapping images (at an acceleration voltage of 15 kV and a probe current of 15 nA): (a) Ni-MOF; (b) CoNi-MOF and (c) Co-MOF.

The first step corresponds to the release of guest molecules, such as ethanol (b.p. = 78 °C) and DMF (b.p. = 153 °C). The second step is caused by the thermal decomposition of the linker molecules. The decomposition temperatures of these MOFs are 298 °C, 412 °C and 425 °C for Co-MOF, CoNi-MOF and Ni-MOF, respectively. Interestingly, the CoNi MOF shows a significantly enhanced thermal stability (more than 100 °C) compared to the pure Co-based MOFs and close to the Ni-based MOF. As thermal stability is important for MOF applications such as heat storage, catalytic processes at high temperatures and so on,[48] this enhanced property of bimetallic MOFs could be interesting. After pyrolysis and annealing, the XRD patterns of MOF derived NiNP@C (Fig. S1a, ESI†) and CoNP@C (Fig. S1b, ESI†) match well with the standard peaks of cubic NiO (JCPDS 65-2901) and cubic Co_3O_4 (JCPDS 43-1003), respectively. Meanwhile, the XRD peaks of the YASNiCo@C can be assigned to the peaks of cubic NiO and cubic Co_3O_4 without any impurities.

N_2 adsorption–desorption isotherms were used to explore the surface area of the resulting catalyst (Fig. 4b). The NiNP@C exhibited a surface area of 36.2 $m^2\ g^{-1}$, which is 79.2% higher than that of CoNP@C (20.2 $m^2\ g^{-1}$). After incorporation of Ni into the frameworks of Co-MOFs, the bimetallic YASNiCo@C catalysts exhibit an enhanced surface area (29.8 $m^2\ g^{-1}$) compared to CoNP@C. As shown in Fig. S2–S4 (ESI†), the hexagonal morphology is maintained during pyrolysis. SEM observation at higher magnification exhibited a porous honeycomb-structure for all of these samples, which is caused by the release of gas (originated from the decomposition of the linkers). These porous honeycomb-structures can provide fast ion transport from the electrolyte to the surface of the active material.[49–53]

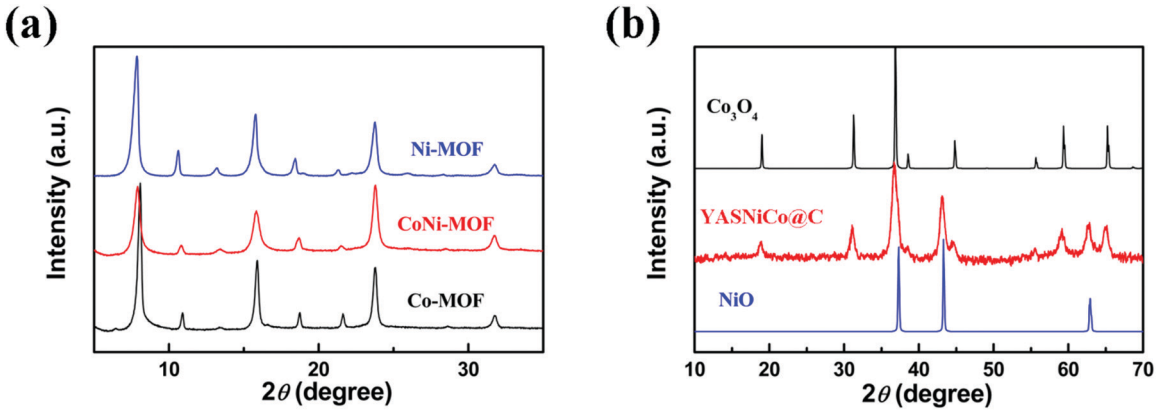

Fig. 3 XRD pattern (using Cu K_α radiation with wave length λ = 0.15405 nm and Ni filter with a step size of 0.02°) of (a) pristine MOFs and (b) YASNiCo@C.

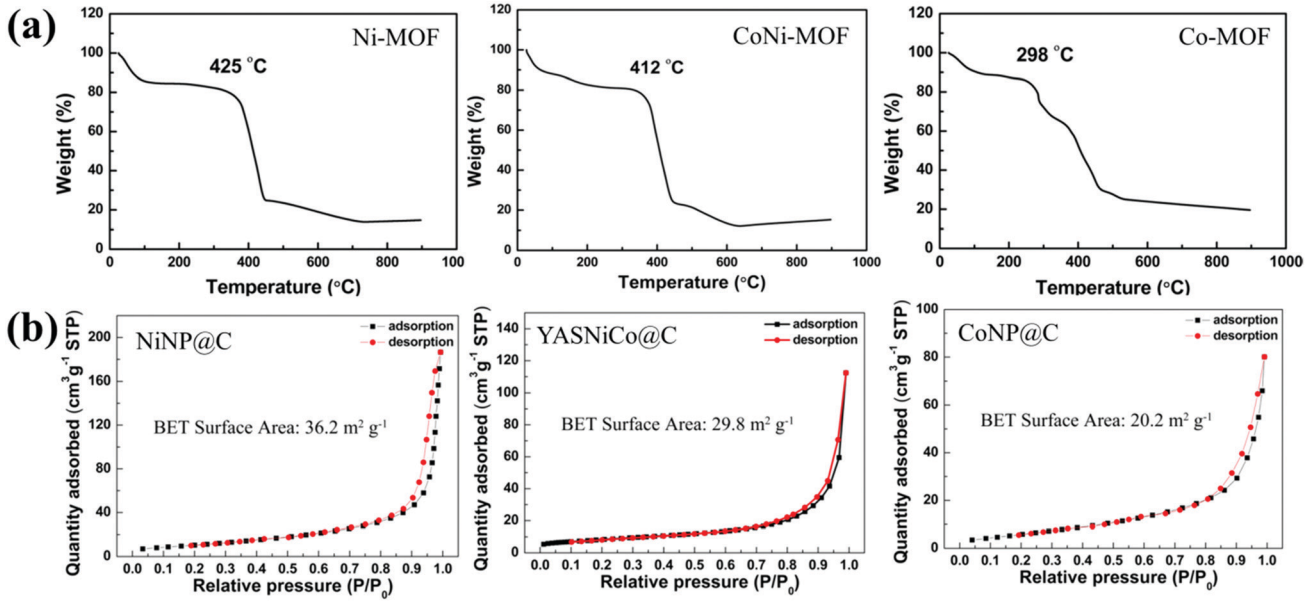

Fig. 4 (a) TGA traces (under an argon atmosphere with a heating rate of 5 °C min^{-1}) of Ni-MOF, CoNi-MOF and Co-MOF. (b) N_2 adsorption–desorption isotherms of NiNP@C, CoNP@C and YASNiCo@C.

To further explore the structure of single nanoparticles, the structure of the MOF-derived catalysts was studied by TEM, HRTEM and STEM-EELS composition maps. Fig. 5 shows that the NiNP@C, CoNP@C and YASNiCo@C samples consisted of nano-particles with irregular morphologies. According to the HRTEM images, the NiNP@C and CoNP@C showed good crystallinity. The magnification of the region marked in yellow and its corresponding power spectrum reveal that the crystal structures are cubic NiO (space group $FM\bar{3}M$) with $a = b = c$ = 4.2000 Å and cubic Co_3O_4 (space group $FD\bar{3}MZ$) with $a = b = c$ = 8.0550 Å, respectively. Both Co_3O_4 and NiO phases are found in the YASNiCo@C sample. The NiO nanostructures are between 10 and 30 nm which is smaller than the CoO nanostructures (40–80 nm) while the Co–Ni oxide particles have a size of 20–40 nm, which is smaller than Co_3O_4 nanostructures. These results are in good agreement with XRD and BET results. The smaller particles could translate into a higher surface area, and more active sides for catalysis. Both Co_3O_4 and NiO phases could be observed for the YASNiCo@C sample. EELS chemical composition maps were used to confirm the elemental distribution of YASNiCo@C. According to the EELS chemical composition maps obtained from the red square region in the HAADF STEM micrograph (Fig. 5c and Fig. S5, S6, ESI†), the coexistence of Ni, Co, O and C in these samples is proven. However, uneven distribution of Co and Ni can be observed by elemental maps in the YASNiCo@C nanostructures. Co preferentially sits on the outside of the particles. A similar phenomenon was observed in the work of Huolin L. Xin *et al.*,[54] where the authors mentioned that it was probably caused by the different diffusion coefficients of Co and Ni in the Ni–Co–O system.[55–57] On the surface of the nanoparticles, there is an ultrathin (around 2 nm thickness) C layer, leading to a yolk–albumen–shell structure. This structure of ultrathin C coating metal oxide particles is a possible highway for electrons to

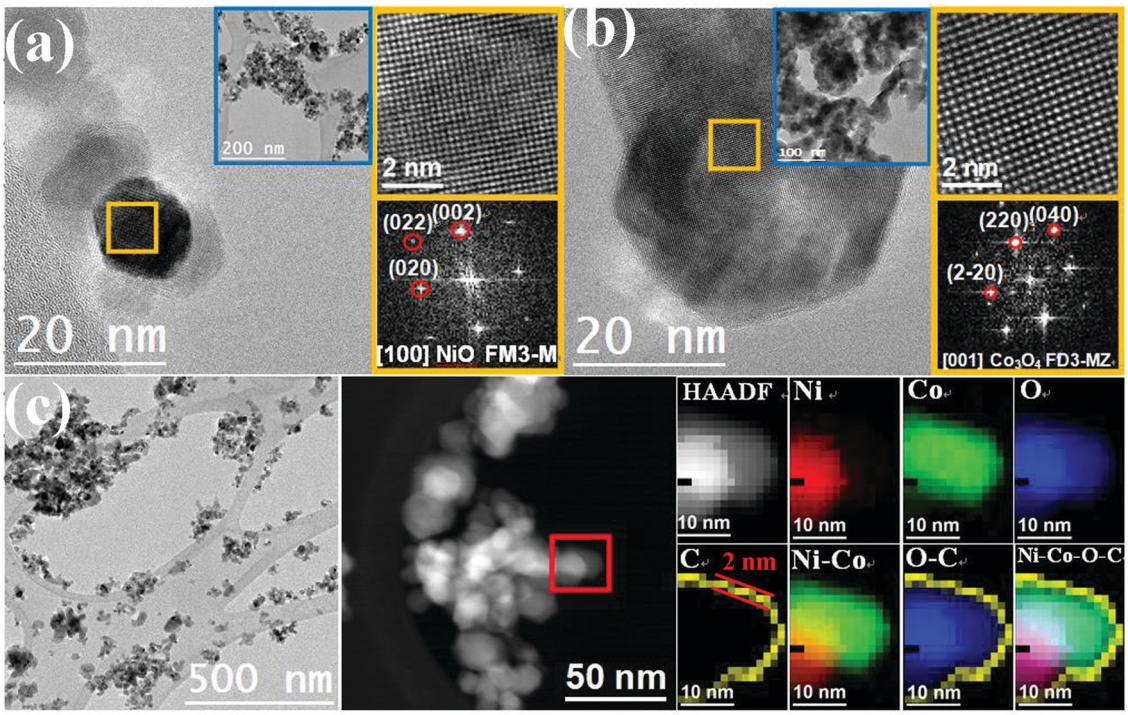

Fig. 5 HRTEM images and the corresponding power spectra (FFT) of (a) NiNP@C and (b) CoNP@C. (c) HRTEM images and EELS chemical composition maps obtained of YASNiCo@C from the area marked by the square in the STEM micrograph. Individual Ni $L_{2,3}$-edges at 855 eV (red), Co $L_{2,3}$-edges at 779 eV (green), O K-edge at 532 eV (blue) and C K-edge at 284 eV (yellow) as well as the composite (Ni–Co, O–C and Ni–O–C) elemental map of this nanostructure.

overcome the low conductivity of the metal oxides. On the other hand, in order to improve the catalytic performance of metal oxide–carbon composite materials, the effective surface area of metal oxide@carbon composite materials should be increased by reducing the particle size and decreasing the thickness of the carbon layer. It can be estimated that the increased surface area and ultrathin carbon layer of YASNiCo@C could facilitate the electrocatalysis performance of YASNiCo@C for glucose oxidation.

For an analytical application, the fabricated MOF-derived materials were used for the detection of glucose using an amperometric method. When 1 mM glucose was added to the 0.1 M NaOH solution, a clear increase of current (at +0.55 V *vs.* Hg/HgO) can be observed for all these samples (Fig. 6a), except for the bare carbon paper (Fig. S7, ESI†). Even though CoNP@C has a much smaller surface area than NiNP@C, the amperometric response of CoNP@C (1.11 mA cm^{-2}) is 76.2% higher than that of NiNP@C (0.63 mA cm^{-2}) for 1 mM glucose. Compared to the single metal-MOF derived materials, the amperometric repsonse of YASNiCo@C (1.82 mA cm^{-2}) is two times higher than that of NiNP@C and 64.0% higher than that of CoNP@C for 1 mM glucose. This might be due to the increase of surface area and/or the synergistic effect of bimetallic oxide. The optimal detection potential of glucose of YASNiCo@C was explored by scanning the potential from +0.45 to +0.6 V *vs.* Hg/HgO in a solution of 1 mM glucose. As shown in Fig. 6b, the response current increases with increasing potential. However, when the potential increased from +0.55 V to +0.6 V *vs.* Hg/HgO, the response current only increased by 7.7%. Considering the influence of interferents and electrolyte polarization (oxygen evolution) at a higher potential, +0.55 V *vs.* Hg/HgO was used for the rest of the tests. At +0.55 V the response currents were recorded while different concentrations of glucose solutions were successively injected into a 0.1 M NaOH solution under stirring with YASNiCo@C as the catalyst (Fig. 6c). Based on these data, the calibration curves are presented in the inset of Fig. 6c. Since the electrochemical oxidation of glucose on the catalyst surface, it is considered as a surface catalytic process. According to previous reports,[58,59] the Langmuir fitting equation can be used to fit the calibration curve. The current (y) is correlated with the glucose concentration (x) in the range of 5–5000 μM with a correlation coefficient of 0.999 by the following equation:

$$y = \frac{6.5237x}{2325.43 + x} \quad (1)$$

Between 5 μM and 1000 μM glucose, a linear relationship can be approximated as:

$$y = 0.07474 + 0.00198x \quad (2)$$

The amperometric response is linear with R^2 = 0.992. In this concentration range, the sensitivity is 1964 μA cm^{-2} mM^{-1}. The detection limit of the YASNiCo@C is 0.75 μM at a signal-to-noise ratio of 3. Compared to other Ni–Co oxide based electrodes reported in the literature, our YASNiCo@C based electrode has a higher sensitivity than most of the recently reported bimetallic metal oxides based on Ni and Co (Table S1, ESI†).

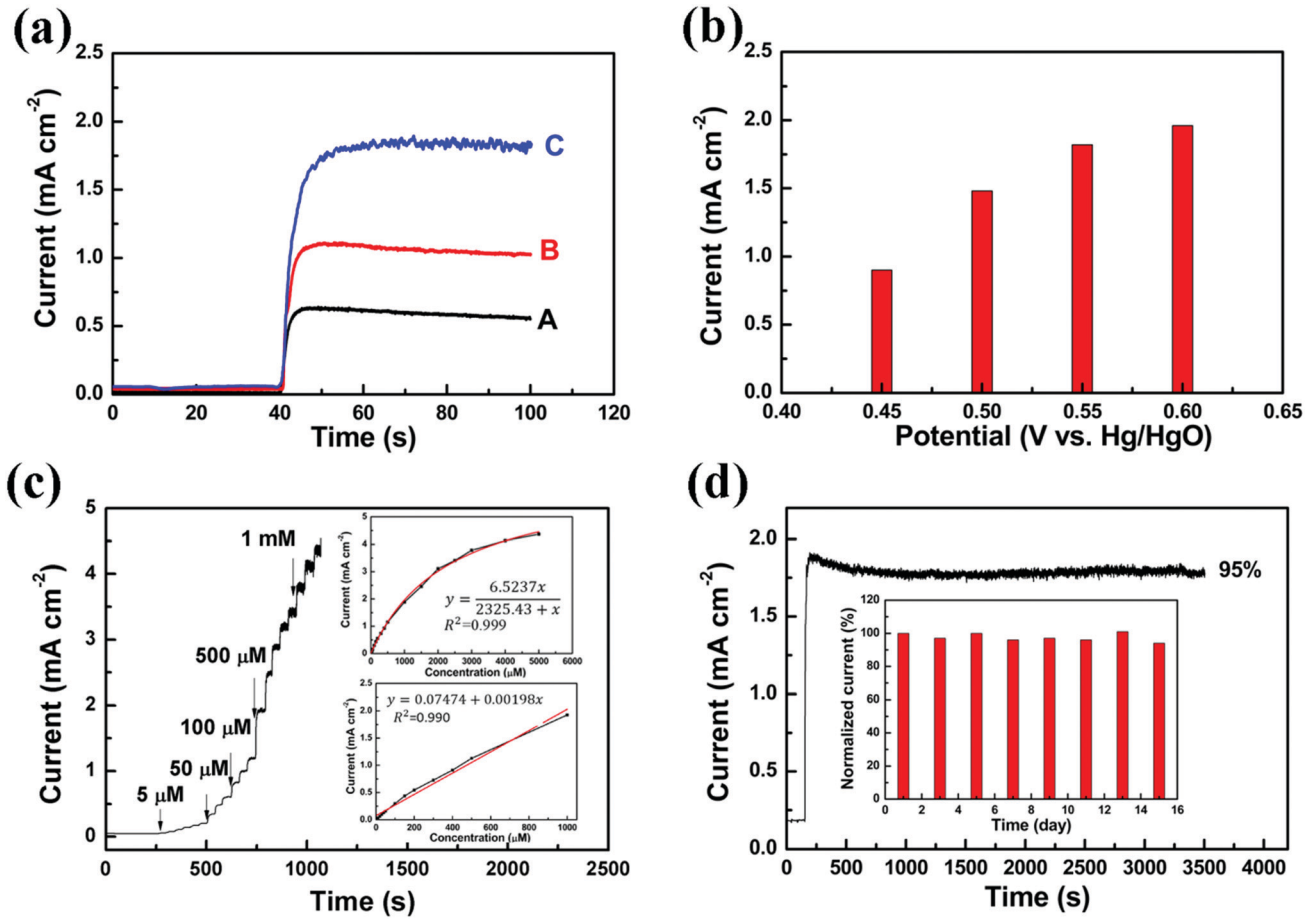

Fig. 6 (a) Amperometric responses of the NiNP@C (A), CoNP@C (B) and YASNiCo@C (C) electrodes to the addition of 1 mM glucose at +0.55 V *vs.* Hg/HgO. (b) Amperometric responses of the YASNiCo@C electrode at potentials from +0.45 V to +0.6 V *vs.* Hg/HgO to the addition of 1 mM glucose. (c) Amperometric response to successive additions of glucose obtained by the YASNiCo@C electrode at an applied potential of 0.55 V *vs.* Hg/HgO, while the inset shows the calibration curve. (d) Long time-stability test for the YASNiCo@C electrode and normalized sensitivity of the YASNiCo@C electrode for glucose measured every two days by amperometric measurement over 15 consecutive days.

The possible electro-oxidation mechanism for glucose oxidation on the YASNiCo@C electrode surface in an alkaline solution is consistent with previous reports as follows (M = Ni or Co):[38,60]

$$M(OOH)_3 + H_2O + e^- \rightleftharpoons M(OH)_2 + OH^- \quad (3)$$

$$2M(OOH)_3 + \text{glucose}(C_6H_{12}O_6, R_1CHOHR_2) \rightarrow 2M(OH)_2 + \text{gluconolactone}(C_6H_{10}O_6, R_1CHOR_2) \quad (4)$$

The reactions (3) occur electrochemically at the target potential (0.55 V). After addition of glucose into the electrolyte, the oxidative M(III) could catalyze glucose oxidation to generate gluconolactone and then gluconolactone is further hydrolyzed to glucose acid.

For the detection of glucose, there are various interferents present in human body fluids, such as ascorbic acid (AA), uric acid (UA), fructose and sucrose. Physiologically relevant concentrations of these interferents were added stepwise to the electrolyte in the following order: glucose (1 mM), UA (60 μM), AA (20 μM), sucrose (15 μM) and fructose (1.62 μM).[61–67] There is no noticable current response for these interferents (Fig. S8, ESI†). The stability of the YASNiCo@C electrode for the detection of glucose was determined by continuous and intermittent tests using 1 mM glucose. After around 1 h of continuous amperometric testing, the current response of the YASNiCo@C electrode retains 95% of the initial response (Fig. 6d). The stability of the YASNiCo@C electrode was also assessed by amperometric measurement every two days during a 15 day period. After 15 days (in ambient atmosphere), the sensitivity of the electrode still retained 94% of its initial response as shown in the inset of Fig. 6d. To investigate the reproducibility of the YASNiCo@C electrode, three different YASNiCo@C electrodes were prepared separately to detect 1 mM glucose. The inter-electrode reproducibility was about 5.4%. In addition, the three YASNiCo@C electrodes exhibit an intra-electrode reproducibility with a relative standard deviation (R.S.D.) of 2.5% (n = 3) for 1 mM glucose. All these results suggest that the YASNiCo@C electrode is an excellent catalytic material for amperometric glucose sensors.

3. Conclusions

In summary, different compositions and structures of Co–Ni metal oxides with ultrathin carbon shell materials were

prepared *via* pyrolysis of bimetallic or single metal based MOFs. Among these materials, the bimetallic MOF derived yolk–albumen–shell structure of the Ni–Co@C composite materials exhibited the highest electrocatalysis performance for glucose oxidation. The good electrocatalytic properties of the YASNiCo@C can be attributed to (1) the large surface area and the presence of an ultrathin carbon layer, (2) a multi-dimensional hierarchical structure and (3) the synergistic effect of the combination of two metal oxides. These results indicate that the YASNiCo@C electrode is a promising candidate for amperometric glucose sensors.

4. Experimental section

Synthesis of bimetallic MOFs

All reagents were of analytical purity and used as received without further purification. The series of MOFs are synthesized by a mild solvothermal method: 3.492 g of $Ni(NO_3)_2{\cdot}6H_2O$ ($\geq$99%, VWR International bvba, Belgium) was dissolved in 40 mL *N*,*N*-dimethylformamide (DMF, $\geq$99% Chem-Lab). 0.844 g 1,3,5-benzenetricarboxylic acid (H_3BTC, 98% purity, ABCR, Germany) and 0.768 g 4,4-dipyridyl (bipy, 98% purity, Acros Organics) were dissolved in 40 mL DMF in a second glass bottle. After mixing of both solutions, the mixture solution was heated to 50 °C in a water bath (Memmert, WNB 45) for 72 h. The resulting products were washed with DMF and ethanol several times, respectively. After removing the residual reactant, the samples were dried in an oven under air at 60 °C overnight. The resulting sample was named as Ni-BTC MOFs. Co-BTC MOFs and Co–Ni–BTC MOFs were synthesized by the same method as described for Ni-BTC MOFs, except that the metal sources were changed to 3.497 g $Co(NO_3)_2{\cdot}6H_2O$ ($\geq$99%, Merck, Germany, for Co-BTC) or a mixture (for Co–Ni–BTC MOFs) of 2.328 g $Ni(NO_3)_2{\cdot}6H_2O$ and 1.164 g $Co(NO_3)_2{\cdot}6H_2O$. The metal ratio of Ni and Co in the CoNi-MOFs is 1 : 1.06, which was determined by ICP-OES analysis after dissolution into 0.5 M HCl.

Preparation of mixed Ni–Co oxide@ultrathin carbon shell

Firstly, the MOF samples were pyrolyzed at 500 °C for 8 h in a nitrogen gas atmosphere (99.998%) with a flow rate of 300 cm^3 min^{-1}. The temperature inside the furnace was gradually increased to 500 °C at a heating rate of 3 °C min^{-1} (the same rate for the cooling procedure). In order to get metal oxide, the resulting powder was further annealed at 350 °C for 3 h under air. These powders were named as NiNP@C, YASNiCo@C and CoNP@C, respectively.

Material characterization

All X-ray diffraction (XRD) data were recorded on a Bruker AXS D8 diffractometer using Cu K_α radiation (wave length λ = 0.15405 nm) and a Ni filter with a step size of 0.02° (1.0 s per step). Thermogravimetric analysis (TGA) tests were analyzed under an argon atmosphere on an AutoTGA 2950HR V5.4A, TA Instruments with platinum pans at a heating rate of 5 °C min^{-1}. The onset temperature of the weight loss in the TGA was used as the decomposition temperature (T_d). The morphologies and microstructures were observed on an FEI/Philips XL30 FEG microscope (SEM) at an acceleration voltage of 15 kV. Chemical composition analyses of MOFs were recorded by a full quantitative electron probe micro-analyzer system coupled with wavelength dispersive spectroscopy (EPMA-WDS; JEOL JXA-8530F, Tokyo, Japan) at an acceleration voltage of 15 kV and a probe current of 15 nA. For the MOF samples, a 10 nm layer of Pt was first sputtered on top of the samples before SEM and EPMA tests. A FEI Tecnai F20 field emission gun microscope was used to collect high resolution transmission electron microscopy (HRTEM) and scanning transmission electron microscopy (STEM) images, operated at 200 kV with a point-to-point resolution of 0.19 nm, equipped with high angle annular dark field (HAADF) and electron energy loss spectroscopy (EELS) detectors. The metal ratios in the CoNi-MOFs were analyzed by inductively coupled plasma optical emission spectroscopy (ICP-OES, Varian 720-ES). Before the ICP test, CoNi-MOF samples were dissolved in 0.5 M HCl. The specific surface area and pore size distributions were investigated by nitrogen adsorption/desorption isotherms by the Brunauer–Emmett–Teller method (BET, Quantachrome Instruments, USA).

Electrochemical measurements

All the electrochemical properties were recorded on an Autolab electrochemical workstation at room temperature in a three-electrode system. The working electrodes were prepared by a dip coating procedure: 10 mg MOF-derived material inks were dispersed into 0.5 mL ethanol (containing 20 μL 5 wt% Nafion, Alfa Aesar Germany). After 30 minutes sonication, 150 μL suspension ink was loaded on the surface of Toray 90 carbon paper (Etek, USA) with a mass loading of about 2 mg cm^{-2}. The as-prepared carbon paper electrode, platinum gauze and a Hg/HgO electrode (Tianjin Aida Hengsheng Technology Co. Ltd, China) were used as the working electrode, the counter electrode and the reference electrode, respectively. Before testing, the working electrode was activated by cycling the potential between 0 V and 0.65 V *vs.* Hg/HgO at a scan rate of 30 mV s^{-1} until the CV curves are stable. All electrochemical experiments were carried out in 0.1 M NaOH.

Conflicts of interest

There are no conflicts to declare.

Acknowledgements

X. Zhang and J. Fransaer acknowledge funding from FWO project (12ZV320N). Funding from Southwest University (SWU019042) is acknowledged. K. Wan is grateful to the Oversea Study Program of Guangzhou Elite Project. M.W. Xu appreciates support from the National Natural Science Foundation of China (No. 21773188). ICN2 acknowledge funding from Generalitat de Catalunya 2017 SGR 327 and the Spanish MINECO project ENE2017-85087-C3. ICN2 is supported by the Severo Ochoa program from Spanish

MINECO (Grant No. SEV-2017-0706) and is funded by the CERCA Programme/Generalitat de Catalunya. Part of the present work has been performed in the framework of Universitat Autònoma de Barcelona Materials Science PhD program. TZ has received funding from the CSC-UAB PhD scholarship program.

References

1 L. C. Clark Jr and C. Lyons, Electrode systems for continuous monitoring in cardiovascular surgery, *Ann. N. Y. Acad. Sci.*, 1962, **102**, 29–45.
2 S. Updike and G. Hicks, The enzyme electrode, *Nature*, 1967, **214**, 986.
3 H. Zhu, L. Li, W. Zhou, Z. P. Shao and X. J. Chen, Advances in non-enzymatic glucose sensors based on metal oxides, *J. Mater. Chem. B*, 2016, **4**, 7333–7349.
4 Z. Zhu, L. Garcia-Gancedo, A. J. Flewitt, H. Xie, F. Moussy and W. I. Milne, A critical review of glucose biosensors based on carbon nanomaterials: carbon nanotubes and graphene, *Sensors*, 2012, **12**, 5996–6022.
5 P. D. Hale, T. Inagaki, H. I. Karan, Y. Okamoto and T. A. Skotheim, A new class of amperometric biosensor incorporating a polymeric electron-transfer mediator, *J. Am. Chem. Soc.*, 1989, **111**, 3482–3484.
6 S. Park, H. Boo and T. D. Chung, Electrochemical non-enzymatic glucose sensors, *Anal. Chim. Acta*, 2006, **556**, 46–57.
7 S. A. Zaidi and J. H. Shin, Recent developments in nanostructure based electrochemical glucose sensors, *Talanta*, 2016, **149**, 30–42.
8 X. H. Niu, X. Li, J. M. Pan, Y. F. He, F. X. Qiu and Y. S. Yan, Recent advances in non-enzymatic electrochemical glucose sensors based on non-precious transition metal materials: opportunities and challenges, *RSC Adv.*, 2016, **6**, 84893–84905.
9 S. Zheng, B. Li, Y. Tang, Q. Li, H. Xue and H. Pang, Ultrathin nanosheet-assembled $[Ni_3(OH)_2(PTA)_2(H_2O)_4]\cdot 2H_2O$ hierarchical flowers for high-performance electrocatalysis of glucose oxidation reactions, *Nanoscale*, 2018, **10**, 13270–13276.
10 W. W. Mao, H. P. He, P. C. Sun, Z. Z. Ye and J. Y. Huang, Three-Dimensional Porous Nickel Frameworks Anchored with Cross-Linked Ni(OH)(2) Nanosheets as a Highly Sensitive Nonenzymatic Glucose Sensor, *ACS Appl. Mater. Interfaces*, 2018, **10**, 15088–15095.
11 C. Zhang, L. H. Qian, K. Zhang, S. L. Yuan, J. W. Xiao and S. Wang, Hierarchical porous Ni/NiO core-shells with superior conductivity for electrochemical pseudo-capacitors and glucose sensors, *J. Mater. Chem. A*, 2015, **3**, 10519–10525.
12 J. N. Xu, F. H. Li, D. D. Wang, M. H. Nawaz, Q. B. An and D. X. Han, *et al.*, Co3O4 nanostructures on flexible carbon cloth for crystal plane effect of nonenzymatic electrocatalysis for glucose, *Biosens. Bioelectron.*, 2019, **123**, 25–29.
13 L. Q. Kang, D. P. He, L. L. Bie and P. Jiang, Nanoporous cobalt oxide nanowires for non-enzymatic electrochemical glucose detection, *Sens. Actuators, B*, 2015, **220**, 888–894.
14 H. X. Dai, M. Lin, N. Wang, F. Xu, D. L. Wang and H. Y. Ma, Nickel-Foam-Supported Co3O4 Nanosheets/PPy Nanowire Heterostructure for Non-enzymatic Glucose Sensing, *ChemElectroChem*, 2017, **4**, 1135–1140.
15 C. Y. Chen, M. Shi, M. W. Xue and Y. J. Hu, Synthesis of nickel(II) coordination polymers and conversion into porous NiO nanorods with excellent electrocatalytic performance for glucose detection, *RSC Adv.*, 2017, **7**, 22208–22214.
16 K. F. Huo, Y. Li, R. S. Chen, B. Gao, C. J. Peng and W. J. Zhang, *et al.*, Recyclable Non-Enzymatic Glucose Sensor Based on $Ni/NiTiO_3/TiO_2$ Nanotube Arrays, *ChemPlusChem*, 2015, **80**, 576–582.
17 T. F. Wang, L. L. Xi and J. L. Wang, In situ fabrication of cobalt nanoflowers on sulfonated and fluorinated poly(arylene ether ketone-benzimidazole) template film for the electrocatalytic oxidation of glucose, *Talanta*, 2018, **178**, 481–490.
18 R. Madhu, V. Veeramani, S. M. Chen, A. Manikandan, A. Y. Lo and Y. L. Chueh, Honeycomb-like Porous Carbon–Cobalt Oxide Nanocomposite for High-Performance Enzyme less Glucose Sensor and Supercapacitor Applications, *ACS Appl. Mater. Interfaces*, 2015, **7**, 15812–15820.
19 J. Balamurugan, T. D. Thanh, G. Karthikeyan, N. H. Kim and J. H. Lee, A novel hierarchical 3D N–Co-CNT@NG nanocomposite electrode for non enzymatic glucose and hydrogen peroxide sensing applications, *Biosens. Bioelectron.*, 2017, **89**, 970–977.
20 L. Bao, T. Li, S. Chen, C. Peng, L. Li and Q. Xu, *et al.*, 3D Graphene Frameworks/$Co3O_4$ Composites Electrode for High-Performance Supercapacitor and Enzymeless Glucose Detection, *Small*, 2017, **13**, 1602077.
21 A. Rengaraj, Y. Haldorai, C. H. Kwak, S. Ahn, K. J. Jeon and S. H. Park, *et al.*, Electrodeposition of flower-like nickel oxide on CVD-grown graphene to develop an electrochemical non-enzymatic biosensor, *J. Mater. Chem. B*, 2015, **3**, 6301–6309.
22 Y. Ni, J. Xu, Q. Liang and S. J. Shao, Enzyme-free glucose sensor based on heteroatom-enriched activated carbon (HAC) decorated with hedgehog-like NiO nanostructures, *Sens. Actuators, B*, 2017, **250**, 491–498.
23 X. Li, J. Wei, Q. Li, S. Zheng, Y. Xu and P. Du, *et al.*, Nitrogen-Doped Cobalt Oxide Nanostructures Derived from Cobalt–Alanine Complexes for High-Performance Oxygen Evolution Reactions, *Adv. Funct. Mater.*, 2018, **28**, 1800886.
24 S. Q. Ci, S. Mao, T. Z. Huang, Z. H. Wen, D. A. Steeber and J. H. Chen, Enzymeless Glucose Detection Based on CoO/Graphene Microsphere Hybrids, *Electroanalysis*, 2014, **26**, 1326–1334.
25 D. Wu, Z. Guo, X. Yin, Q. Pang, B. Tu and L. Zhang, *et al.*, Metal–organic frameworks as cathode materials for $Li–O_2$ batteries, *Adv. Mater.*, 2014, **26**, 3258–3262.
26 F. Zou, X. Hu, Z. Li, L. Qie, C. Hu and R. Zeng, *et al.*, MOF-Derived Porous ZnO/ZnFe2O4/C Octahedra with Hollow Interiors for High-Rate Lithium-Ion Batteries, *Adv. Mater.*, 2014, **26**, 6622–6628.
27 X. Zhang, J. Luo, P. Tang, X. Ye, X. Peng and H. Tang, *et al.*, A universal strategy for metal oxide anchored and binder-free carbon matrix electrode: A supercapacitor case with

superior rate performance and high mass loading, *Nano Energy*, 2017, **31**, 311–321.

28 R. R. Salunkhe, Y. V. Kaneti and Y. Yamauchi, Metal–organic framework-derived nanoporous metal oxides toward supercapacitor applications: progress and prospects, *ACS Nano*, 2017, **11**, 5293–5308.

29 X. Jiang, H. Li, S. Li, S. Huang, C. Zhu and L. Hou, Metal-organic framework-derived Ni–Co alloy@ carbon microspheres as high-performance counter electrode catalysts for dye-sensitized solar cells, *Chem. Eng. J.*, 2018, **334**, 419–431.

30 S.-H. Hsu, C.-T. Li, H.-T. Chien, R. R. Salunkhe, N. Suzuki and Y. Yamauchi, *et al.*, Platinum-free counter electrode comprised of metal-organic-framework (MOF)-derived cobalt sulfide nanoparticles for efficient dye-sensitized solar cells (DSSCs), *Sci. Rep.*, 2014, **4**, 6983.

31 X. Zhang, J. Luo, H.-F. Lin, P. Tang, J. R. Morante and J. Arbiol, *et al.*, Tailor-made metal–nitrogen–carbon bifunctional electrocatalysts for rechargeable Zn-air batteries *via* controllable MOF units, Energy Storage, *Materials*, 2019, **17**, 46–61.

32 X. Zhang, J. Luo, K. Wan, D. Plessers, B. Sels and J. Song, *et al.*, From rational design of a new bimetallic MOF family with tunable linkers to OER catalysts, *J. Mater. Chem. A*, 2019, **7**, 1616–1628.

33 S. Gadipelli, T. Zhao, S. A. Shevlin and Z. Guo, Switching effective oxygen reduction and evolution performance by controlled graphitization of a cobalt–nitrogen–carbon framework system, *Energy Environ. Sci.*, 2016, **9**, 1661–1667.

34 X. Xiao, Q. Li, X. Yuan, Y. Xu, M. Zheng and H. Pang, Ultrathin nanobelts as an excellent bifunctional oxygen catalyst: insight into the subtle changes in structure and synergistic effects of bimetallic metal–organic framework, Small, *Methods*, 2018, **2**, 1800240.

35 H. Zhou, M. Zheng, H. Tang, B. Xu, Y. Tang and H. Pang, Amorphous Intermediate Derivative from ZIF-67 and Its Outstanding Electrocatalytic Activity, *Small*, 2020, **16**, 1904252.

36 L. B. Shi, Y. F. Li, X. Cai, H. L. Zhao and M. B. Lan, ZIF-67 derived cobalt-based nanomaterials for electrocatalysis and nonenzymatic detection of glucose: Difference between the calcination atmosphere of nitrogen and air, *J. Electroanal. Chem.*, 2017, **799**, 512–518.

37 X. X. Duan, K. L. Liu, Y. Xu, M. T. Yuan, T. Gao and J. Wang, Nonenzymatic electrochemical glucose biosensor constructed by NiCo2O4@ Ppy nanowires on nickel foam substrate, *Sens. Actuators, B*, 2019, **292**, 121–128.

38 J. Yang, M. Cho and Y. Lee, Synthesis of hierarchical NiCo2O4 hollow nanorods *via* sacrificial-template accelerate hydrolysis for electrochemical glucose oxidation, *Biosens. Bioelectron.*, 2016, **75**, 15–22.

39 V. Archana, Y. Xia, R. Y. Fang and G. G. Kumar, Hierarchical CuO/NiO–Carbon Nanocomposite Derived from Metal Organic Framework on Cello Tape for the Flexible and High Performance Nonenzymatic Electrochemical Glucose Sensors, *ACS Sustainable Chem. Eng.*, 2019, **7**, 6707–6719.

40 B. Chen, G. Ma, Y. Zhu, J. Wang, W. Xiong and Y. Xia, Metal-organic-framework-derived bi-metallic sulfide on N, S-codoped porous carbon nanocomposites as multifunctional electrocatalysts, *J. Power Sources*, 2016, **334**, 112–119.

41 M. A. Gotthardt, R. Schoch, S. Wolf, M. Bauer and W. Kleist, Synthesis and characterization of bimetallic metal-organic framework Cu-Ru-BTC with HKUST-1 structure, *Dalton Trans.*, 2015, **44**, 2052–2056.

42 W. Guo, W. Xia, K. Cai, Y. Wu, B. Qiu and Z. Liang, *et al.*, Kinetic-Controlled Formation of Bimetallic Metal–Organic Framework Hybrid Structures, *Small*, 2017, **13**, 1702049.

43 A. Schejn, A. Aboulaich, L. Balan, V. Falk, J. Lalevée and G. Medjahdi, *et al.*, Cu^{2+}-doped zeolitic imidazolate frameworks (ZIF-8): efficient and stable catalysts for cycloadditions and condensation reactions, *Catal. Sci. Technol.*, 2015, **5**, 1829–1839.

44 H. Yang, X.-W. He, F. Wang, Y. Kang and J. Zhang, Doping copper into ZIF-67 for enhancing gas uptake capacity and visible-light-driven photocatalytic degradation of organic dye, *J. Mater. Chem.*, 2012, **22**, 21849.

45 J. A. Botas, G. Calleja, M. Sanchez-Sanchez and M. G. Orcajo, Cobalt doping of the MOF-5 framework and its effect on gas-adsorption properties, *Langmuir*, 2010, **26**, 5300–5303.

46 P. Kuisma-Kursula, Accuracy, precision and detection limits of SEM-WDS, SEM-EDS and PIXE in the multi-elemental analysis of medieval glass, *X-Ray Spectrom.*, 2000, **29**, 111–118.

47 Y. Li, L. Xie, Y. Liu, R. Yang and X. Li, Favorable hydrogen storage properties of M (HBTC)(4,4′-bipy)·3DMF (M = Ni and Co), *Inorg. Chem.*, 2008, **47**, 10372–10377.

48 A. J. Howarth, Y. Liu, P. Li, Z. Li, T. C. Wang and J. T. Hupp, *et al.*, Chemical, thermal and mechanical stabilities of metal–organic frameworks, *Nat. Rev. Mater.*, 2016, **1**, 1–15.

49 S. Chen and S.-Z. Qiao, Hierarchically porous nitrogen-doped graphene–NiCo2O4 hybrid paper as an advanced electrocatalytic water-splitting material, *ACS Nano*, 2013, **7**, 10190–10196.

50 X. Gao, H. Zhang, Q. Li, X. Yu, Z. Hong and X. Zhang, *et al.*, Hierarchical NiCo2O4 Hollow Microcuboids as Bifunctional Electrocatalysts for Overall Water-Splitting, *Angew. Chem.*, 2016, **128**, 6398–6402.

51 X. Lu and C. Zhao, Electrodeposition of hierarchically structured three-dimensional nickel-iron electrodes for efficient oxygen evolution at high current densities, *Nat. Commun.*, 2015, **6**, 6616.

52 C. Ouyang, X. Wang, C. Wang, X. Zhang, J. Wu and Z. Ma, *et al.*, Hierarchically Porous Ni3S2 Nanorod Array Foam as Highly Efficient Electrocatalyst for Hydrogen Evolution Reaction and Oxygen Evolution Reaction, *Electrochim. Acta*, 2015, **174**, 297–301.

53 C. Xiao, Y. Li, X. Lu and C. Zhao, Bifunctional Porous NiFe/NiCo2O4/Ni Foam Electrodes with Triple Hierarchy and Double Synergies for Efficient Whole Cell Water Splitting, *Adv. Funct. Mater.*, 2016, **26**, 3515–3523.

54 L. Han, Q. Meng, D. Wang, Y. Zhu, J. Wang and X. Du, *et al.*, Interrogation of bimetallic particle oxidation in three dimensions at the nanoscale, *Nat. Commun.*, 2016, **7**, 13335.

55 B. Million and J. Kucera, Concentration dependence of diffusion of cobalt in nickel-cobalt alloys, *Acta Metall.*, 1969, **17**, 339–344.

56 M. L. Volpe and J. Reddy, Cation Self-Diffusion and Semiconductivity in NiO, *J. Chem. Phys.*, 1970, **53**, 1117–1125.

57 W. Chen, N. Peterson and W. Reeves, Isotope effect for cation self-diffusion in CoO crystals, *Phys. Rev.*, 1969, **186**, 887.
58 S. Q. Ci, T. Z. Huang, Z. H. Wen, S. M. Cui, S. Mao and D. A. Steeber, *et al.*, Nickel oxide hollow rnicrosphere for non-enzyme glucose detection, *Biosens. Bioelectron.*, 2014, **54**, 251–257.
59 H. Wu, Y. Yu, W. Y. Gao, A. Gao, A. M. Qasim and F. Zhang, *et al.*, Nickel plasma modification of graphene for high-performance non-enzymatic glucose sensing, *Sens. Actuators, B*, 2017, **251**, 842–850.
60 Z. Y. Yu, H. J. Li, X. M. Zhang, N. K. Liu, W. L. Tan and X. Zhang, *et al.*, Facile synthesis of NiCo2O4@Polyaniline core-shell nanocomposite for sensitive determination of glucose, *Biosens. Bioelectron.*, 2016, **75**, 161–165.
61 K. Dhara, J. Stanley, T. Ramachandran, B. G. Nair and S. B. TG, Pt-CuO nanoparticles decorated reduced graphene oxide for the fabrication of highly sensitive non-enzymatic disposable glucose sensor, *Sens. Actuators, B*, 2014, **195**, 197–205.
62 J. Dong, L. Ren, Y. Zhang, X. Cui, P. Hu and J. Xu, Direct electrodeposition of cable-like CuO@Cu nanowires array for non-enzymatic sensing, *Talanta*, 2015, **132**, 719–726.
63 H. Huo, Y. Zhao and C. Xu, 3D Ni_3S_2 nanosheet arrays supported on Ni foam for high-performance supercapacitor and non-enzymatic glucose detection, *J. Mater. Chem. A*, 2014, **2**, 15111–15117.
64 C.-W. Kung, Y.-H. Cheng and K.-C. Ho, Single layer of nickel hydroxide nanoparticles covered on a porous Ni foam and its application for highly sensitive non-enzymatic glucose sensor, *Sens. Actuators, B*, 2014, **204**, 159–166.
65 H. Liu, X. Wu, B. Yang, Z. Li, L. Lei and X. Zhang, Three-dimensional porous NiO nanosheets vertically grown on graphite disks for enhanced performance non-enzymatic glucose sensor, *Electrochim. Acta*, 2015, **174**, 745–752.
66 G.-X. Zhong, W.-X. Zhang, Y.-M. Sun, Y.-Q. Wei, Y. Lei and H.-P. Peng, *et al.*, A nonenzymatic amperometric glucose sensor based on three dimensional nanostructure gold electrode, *Sens. Actuators, B*, 2015, **212**, 72–77.
67 Z. Zhuang, X. Su, H. Yuan, Q. Sun, D. Xiao and M. M. Choi, An improved sensitivity non-enzymatic glucose sensor based on a CuO nanowire modified Cu electrode, *Analyst*, 2008, **133**, 126–132.